Progress in PHOTOVOLTAICS

PROGRESS IN PHOTOVOLTAICS: RESEARCH AND APPLICATIONS
Prog. Photovolt: Res. Appl. 2015; **23**:238–246
Published online 21 September 2013 in Wiley Online Library (wileyonlinelibrary.com). DOI: 10.1002/pip.2421

RESEARCH ARTICLE

Patterning of organic photovoltaic modules by ultrafast laser

Peter Kubis[1,3]*, Ning Li[1], Tobias Stubhan[1], Florian Machui[1], Gebhard J. Matt[1], Monika M. Voigt[1,2] and Christoph J. Brabec[1,2]

[1] Institute of Materials for Electronics and Energy Technology (i-MEET), Friedrich-Alexander-University Erlangen-Nuremberg, Martensstrasse 7, 91058 Erlangen, Germany
[2] Bavarian Center for Applied Energy Research (ZAE Bayern), Haberstr. 2a, 91058 Erlangen, Germany
[3] Erlangen Graduate School in Advanced Optical Technologies (SAOT), Paul-Gordan-Str. 6, 91052 Erlangen, Germany

ABSTRACT

In this paper, we demonstrate that laser patterning of organic solar cells by ultrafast laser systems (pulse length <350 fs) is an attractive process to produce photovoltaic modules with outstanding high geometric fill factors. Moreover, in terms of precision, registration, and debris generation and in terms of keeping the damage to the underneath layers at a minimum, ultrafast laser patterning with a pulse length of few hundreds of femtoseconds turns out to yield superior results. Ablation of all three different solar cell layers (electrodes (P1 and P3) and interfaces and semiconductor (P2)) is achieved with a single wavelength simply by a precise adjustment of the laser fluence and the patterning overlap. Camera positioning allows a precise registration between the various processing steps and a reduction of the width of the overall interconnection regime to the hundreds of micrometers dimension, resulting in high geometrical fill factors of over 90% for monolithically interconnected organic solar cell modules. Copyright © 2013 John Wiley & Sons, Ltd.

KEYWORDS

femtosecond pulses; laser patterning; PV module; organic solar cells

***Correspondence**

Peter Kubis, Institute of Materials for Electronics and Energy Technology (i-MEET), Friedrich-Alexander-University Erlangen-Nuremberg, Martensstrasse 7, 91058 Erlangen, Germany.
E-mail: peter.kubis@ww.uni-erlangen.de

Received 2 November 2012; Revised 19 July 2013; Accepted 14 August 2013

1. INTRODUCTION

Recent developments in organic photovoltaics (OPV) showed solar cell efficiencies exceeding 10% [1,2], which is already comparable with the class of amorphous and microcrystalline silicon solar cells. Despite the fact that these achievements were obtained under laboratory conditions, OPV is becoming an attractive technology for the consumer electronics and outdoor photovoltaic (PV) market. The ability of solution processing opens the way for variable production schemes utilizing high throughput roll-to-roll (R2R) or inkjet sheet-to-sheet production of OPV cells [3]. The advantages of the various solution processing methods were already discussed for poly(3-hexylthiophene) (P3HT)/[6,6]-phenyl-C_{61}-butyric acid methyl ester (PCBM) composites [4]. Besides inkjet printing, slot die and roller coating techniques were the most frequently demonstrated production methods. On the other hand, thin-film PV modules require the sectioning into multiple cells for series interconnection. The P1 line separates the substrate electrode (indium tin oxide (ITO) in our case), the P2 line removes the semiconductor from the ITO to allow the formation of a low ohmic contact between the top and bottom electrodes, and finally, the P3 line separates the top electrode between the single cells (Figure 1). The area between the P1 and P3 lines is PV inactive, or so-called "dead area". Typically, the dead area is accounted for the module efficiency by the geometrical fill factor (GFF), which is the ratio between the PV active area and the total module area. The larger the dead area, the smaller the GFF and the lower the module efficiency. Consequently, high GFF modules require highest resolution of the P1, P2, and P3 lines. This is a clear bottleneck for slot die or roller coating methods. While both methods allow the deposition of stripe patterns in down-web direction, the resolution is rather in the millimeter regime than in the micrometer regime. As a consequence, most coated modules published so far had a GFF ranging from 50% to approximately 70% including contact areas and bus bars [2,3]. To point out the importance of a high GFF: GFF of 50% reduces a 5% cell into a 2.5% module.

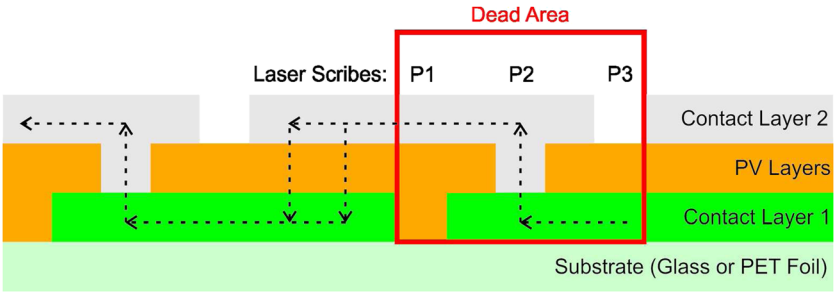

Figure 1. Cross section of the monolithic interconnection. Patterning lines are labeled with P1 (separation of the transparent electrode), P2 (opening in absorber for the interconnection between two electrodes), and P3 (separation of the top electrode). The interconnection region is inactive as a solar cell (dead area).

Thin-film laser processing with picosecond and femtosecond pulsed laser sources developed rapidly during the last years, mainly driven by applications in thin-film PV cells and display technology [5–11]. On the one hand, the laser systems became more and more reliable, operating for thousands of hours without the necessity of service. On the other hand, the dramatic cost decrease of the short pulse laser systems triggered their vast distribution in many areas of thin-film processing. Because of very short interaction time scales between the laser pulse and the material, the ablation process with femtosecond laser pulses can be considered as a direct solid–vapor (solid–plasma) transition. In this case, the lattice is heated on a picosecond time scale, which results in the creation of vapor and plasma phases followed by a rapid expansion into vacuum. During all these processes, thermal heating and heat conduction of the surrounding material can be neglected [14]. These advantages of femtosecond laser pulses allow very precise and pure laser processing of solids without collateral damages to the surrounding layers and layers lying beneath. High ablation efficiency and accuracy of various materials were already demonstrated [12,14–17].

Laser patterning of other thin-film solar cells such as amorphous silicon or copper indium gallium diselenide was intensely investigated [5–9], but little was reported about laser patterning of organic PV modules [18,19]. Assuming good laser beam quality ($M^2 < 1.2$) and femtosecond pulse durations, pulse energies between 1 and 10 µJ on a typical spot size with 30 µm diameter are expected to be sufficient to exceed the ablation threshold of all materials used in OPV. This suggests that patterning of OPV modules with tens of micrometer resolution at scan speeds of several meters per second should be possible. Summarizing all these technical benefits of ultra short pulse laser patterning, we expect that the introduction of laser patterning into the OPV module fabrication technology will have a rapid impact on the commercialization of this young PV technology.

2. MATERIALS AND METHODS

2.1. Laser source

All laser patterning was carried out with an LS 7xxP setup built by LS Laser Systems GmbH (München, Germany). The heart of the system is a femtoREGEN^{TM} UC-1040–8000 fs Yb SHG from High Q Laser GmbH (Rankweil, Austria) emitting at 1040 nm (fundamental wavelength) and 520 nm (first harmonic wavelength) with a pulse duration of <350 fs at repetition rates up to 960 kHz. Maximum pulse energies of 16 µJ (1040 nm) or 6.4 µJ (520 nm) are reached at 500 kHz. The beam quality of the laser system is $M^2 < 1.25$ (1040 nm), $M^2 < 1.5$ (520 nm), and the pulse-to-pulse stability is <2% for both wavelengths. A variable beam expander expands the beam from two to eight times. A galvanometer-mounted mirror deflects the beam over the sample surface with a speed of up to 4000 mm/s. The scanner's objective has a focal length of 330 mm and a focused spot diameter of 32 ± 1 µm (at $1/e^2$ intensity). The power of the laser was measured with the VEGA DISPLAY and sensor 30A-BB-SH-18 ROHS from Ophir Optronics (Jerusalem, Israel).

峰值功率=单脉冲能量/脉冲宽度

2.2. Organic photovoltaic module processing

Inverted PV devices were processed and characterized in ambient atmosphere as reported elsewhere [20]. The layer sequence of all devices was ITO/aluminum-doped ZnO (AZO)/P3HT : PCBM/poly(3,4-ethylenedioxythiophene) (PEDOT) : poly(styrenesulfonate) (PSS)/Ag. ITO-coated glass substrates were patterned with a laser fluence of 0.55 J/cm^2 and 90% overlap (Gaussian beam diameter at $1/e^2$ intensity was assumed for overlap computation) at the first harmonic wavelength (520 nm). After P1 patterning (electrical isolation of transparent electrode), ITO glasses were subsequently cleaned in an ultrasonic bath in acetone and isopropyl alcohol for 10 min each. After drying, the substrates were coated with an AZO precursor via doctor blading. Conversion of the AZO precursors to AZO via hydrolysis was carried out by heating the samples to 140 °C for 5 min. P3HT Lisicon SP 001 batch EE 99602 purchased from Merck Germany and [60]PCBM (technical grade 99%) from Solenne BV, The Netherlands, were separately dissolved in chlorobenzene (99.5%) from Carl Roth Germany at a concentration of 2 wt% and stirred for at least 1 h at 60 °C before being blended in a volume ratio of 1:1. The blended solution was stirred for at least another

hour at 60 °C before use. The P3HT : PCBM active layer was deposited via doctor blading to a thickness of approximately 100 nm. PEDOT : PSS (Clevios P VP Al4083) from H.C. Starck Germany was diluted in isopropyl alcohol (1:5 volume ratio) before it was deposited via doctor blading. After drying, all three layers had to be removed to generate the P2 line (opening in absorber for the interconnection between two electrodes). Patterning of the P2 line is a critical process step, because insufficient removal of all three layers will lead to high ohmic resistance, while too high laser power will cause damage to the underlying ITO. The scribing of the P2 lines was carried out with the laser fluence of 0.27 J/cm^2 and 90% overlap at the first harmonic wavelength (520 nm). Then, the samples were transferred into a nitrogen-filled glove box and annealed at 140 °C for 5 min. A 150-nm-thick Ag layer was thermally evaporated to form the top electrode. The scribing of P3lines, required to separate the Ag electrodes, was carried out with the fluence of 0.57 J/cm^2 and 66.6% overlap again at the first harmonic wavelength (520 nm). The active area of the investigated devices was 30 mm^2 for the reference cells and 115 mm^2 for the modules. Modules consisted of 10 cells connected in series. Current density–voltage (j–V) characteristics were measured with a source measurement unit from BoTest (Wertheim, Germany). Illumination was provided by an Oriel Sol 1A Solarsimulator with AM1.5G spectra at 0.1 W/cm^2 from Newport (Irvine, USA).

3. RESULTS/DISCUSSION

All experiments were carried out by direct ablation [13,21]. First, we experimentally determined the single-shot ablation threshold of all three layers. This was carried out on the separate samples prepared in the same way as the OPV modules. The experimental determination of a material's ablation threshold is described in all details in the literature [13,22,23]. We determined the ablation threshold fluence F_{th} from the relationship between the squared diameter of the ablated spot D^2 and the laser fluence F:

$$D^2 = 2w_0^2 ln\left(\frac{F}{F_{th}}\right) \quad (1)$$

where w_0 is the radius of the laser beam at the 1/e^2 intensity at the surface. The diameters of ablated spots were measured with the optical microscope. Because the pulse energy E is simpler to access (measured output power of the laser divided by the frequency), we substitute the (F/F_{th}) ratio with the (E/E_{th}):

$$D^2 = 2w_0^2 ln\left(\frac{E_{pulse}}{E_{th}}\right) \quad (2)$$

w_0 can now be determined by the slope of a linear fit to D^2 over E_{th} in a semi-logarithmic plot [13]. The ablation threshold fluence is computed from the following:

$$F_{th} = \frac{2E_{th}}{\pi w_0^2} \quad (3)$$

Figure 2 shows the ablation diagrams for ITO, Ag, and AZO/P3HT : PCBM/PEDOT : PSS. The good quality of the linear fit in the semi-logarithmic plots validates the procedure to determine the ablation threshold. Table I summarizes the ablation threshold fluences for all three material systems. Figure 2 is essential to define the process window for the individual layers. For instance, one can immediately tell the laser fluence values that are sufficient to remove the active layer but are still low enough to cause no damage to ITO.

One of the more relevant processing parameters besides fluence and laser wavelength is the overlap. Our strategy to determine the overlap was initially motivated by optimizing the throughput. A series of trials, starting from 10% overlap all the way to 90% overlap, was evaluated for the various layers. Complete ablation was typically observed

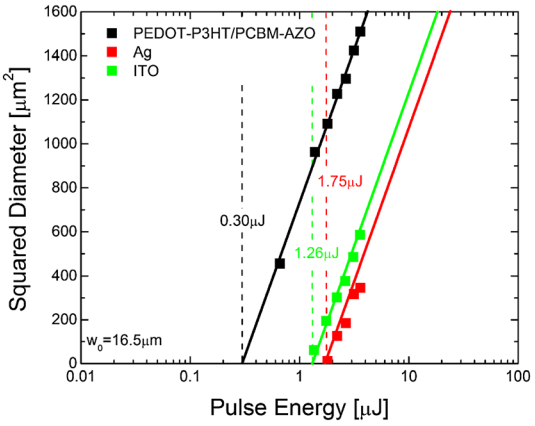

Figure 2. Single-shot ablation threshold measurements of all layers used in our OPV solar cell structure. Squared diameter D^2 of ablated area is plotted as a function of the pulse energy. The slope of the linear fit gives the beam radius on the surface of the layer at the energy intensity of 1/e^2. The extrapolation to zero gives the ablation threshold energy of one pulse.

Table I. Values of the single pulse ablation threshold fluences obtained from the experiment.

Layer	Threshold fluence (J/cm^2)
ITO	0.29
Absorber	0.07
Ag	0.41

The relatively big gap between the threshold fluence of absorber and the transparent indium tin oxide (ITO) provides us with a big process window.

at overlap ratios of 50% or less; however, to guarantee the highest yield, we finally decided to pattern the single stacks with an overlap between 66% and 90%.

3.1. P1 patterning

Ablation of ITO starts at a fluence value of 0.29 J/cm^2. A series of experiments varying laser fluence and overlap was designed to optimize the processing speed while keeping the patterning yield high. The final assessment for the patterning suggested a fluence of 0.55 J/cm^2 together with an overlap of 90%. These parameters allowed complete ablation of ITO (this was proved with the resistivity measurement of >2 MΩ) without the formation of protrusions on the margins, as seen by the atomic force microscopy (AFM) scans depicted in Figure 3. Further, AFM scans prove that no ITO spikes remain on the bottom (this confirmed our assumption after the resistivity measurement that the ITO was totally ablated) as well as on the sides of the grooves. This is important to prevent shunting between the top electrode and the bottom electrode. The groove has got the V shape in the first half of the thickness. This is due to the Gaussian profile of the beam. The energy in this region was not sufficient for the ablation of ITO in whole thickness. Overall, the width of the groove was determined to be 11 µm, an exceptionally low value for a P1 line.

3.2. P2 patterning

P2 patterning required to ablate a stack of three different materials with quite different mechanical properties: AZO, a metal oxide, and two organic layers (P3HT : PCBM and PEDOT : PSS) could be removed in a single step with a laser fluence of 0.27 J/cm^2 (threshold fluence 0.07 J/cm^2; Table I). This was the maximum laser fluence available for processing (fluence between the ablation threshold of AZO/P3HT : PCBM/PEDOT : PSS and ITO, see process window in Figure 2), which did not damage ITO. The absorber stack AZO/P3HT : PCBM/PEDOT : PSS is around 180–200 nm thick. The ablation threshold of the absorber stack is an average number reflecting the material properties of the stack of the individual layers. However, looking at the lateral patterning profile, which is widest for the top layer and smallest for the bottom layer, it becomes clear that the uppermost layer majorly dominates the overall ablation threshold of the stack. It is important to note that the fluence chosen for the P2 patterning was slightly lower (0.27 J/cm^2) than the ablation threshold fluence for the ITO layer lying beneath. This is necessary to prevent ITO damage during P2 patterning. Furthermore, different overlaps with this fluence were proved, and the value of 90% was selected as the most promising one. The AFM scans in Figure 4 proved that the whole layer was ablated with a single-process step.

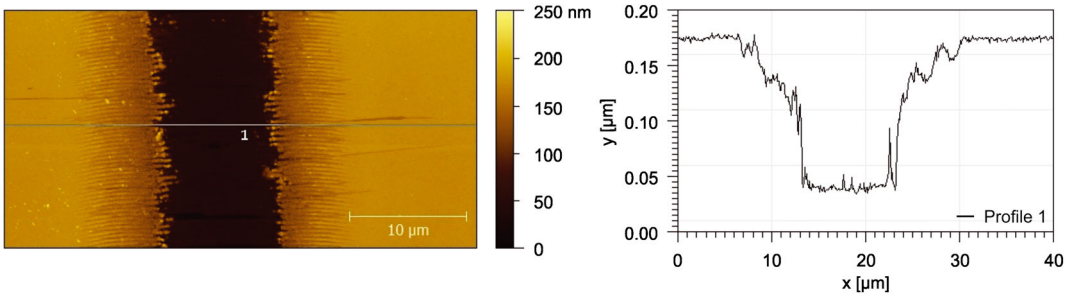

Figure 3. AFM scan of a P1 patterning line in ITO. ITO was completely ablated without the creation of any spikes on the groove edges and without the creation of any debris outside the patterning area.

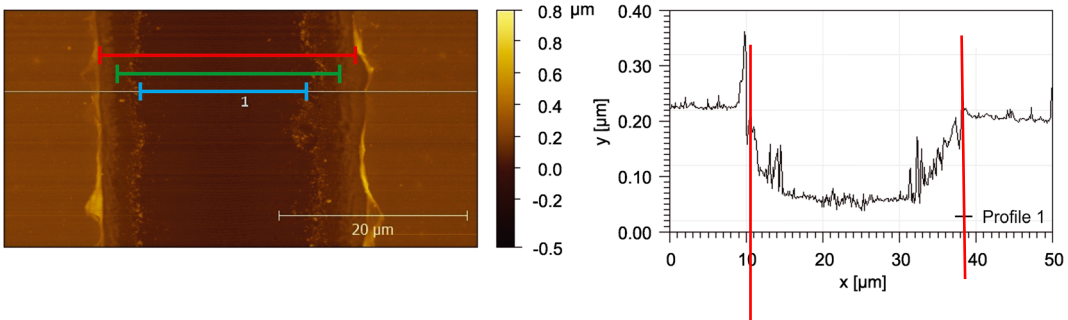

Figure 4. AFM scan of a P2 patterning line in the AZO/P3HT : PCBM/PEDOT : PSS absorber stack. The groove depth perfectly corresponds to the thickness of the absorber. Oblique walls within the groove indicate three steps, also seen in the microscope pictures, indicating the slightly different ablation threshold of the individual absorber materials (AZO, P3HT : PCBM, and PEDOT : PSS) as well as the laser intensity distribution within the stack.

The width of the groove (area close to the ITO) was 17 µm at the bottom. One can recognize three steps on the oblique groove walls (Figure 4, microscope pictures), each indicating one of the three different material layers (AZO/P3HT : PCBM/PEDOT : PSS). From Figure 4, it is also clear that on some locations on the groove edges, the debris can be seen. It is very likely that the formation of this debris is from the uppermost layer (PEDOT : PSS) because the used laser fluence was highly exceeding the ablation threshold fluence of this material.

3.3. P3 patterning

The patterning of the P3 line was carried out directly after evaporation of a silver electrode with a laser fluence of 0.57 J/cm^2 and 66.6% overlap. The AFM profile in Figure 5 shows that by using these process parameters, the resulting groove is deeper than 150 nm (i.e., the thickness of the evaporated silver layer), indicating that this set of parameters not only ablates the Ag layer but also removes parts of the underneath layers (either PEDOT : PSS or P3HT : PCBM/PEDOT : PSS). In any case, the separation of the Ag layer was sufficient, and the electrical isolation between individual cells was perfect (resistivity measurement >2 MΩ). Therefore, we conclude that there is no silver in the groove or, if there is some remaining, it does not bridge the edges of the trench. The width of the groove is more than 11 µm (comparable with the groove width in ITO); however, strong protrusions were found on the margins of the groove, most likely consisting of Ag. These protrusions could be molten silver, which can be generated in the region of Gaussian beam with lower intensity. Because the protrusions occur at the top electrode, no negative impacts on the device performance are expected.

3.4. Modules

First, device trials started with the fabrication of modules consisting only from three monolithically interconnected cells. The module was manufactured by sectioning a small area lab cell with an active area of 10.4 mm^2 (processed on the glass substrates coated with the ITO, with a dimension of 25 × 25 mm) into three individual cells with approximately 3.5 mm^2 (P1 line) and by monolithically interconnecting them in series (P2 and P3 lines). Our standard substrates featuring six cells with 10.4 mm^2 were redesigned to now feature four modules and two reference cells, again each with 10.4 mm^2.

As mentioned earlier, each process step during module patterning has its own functionality. While the P1 and P3 lines are most critical in terms of shunting and shunt-related losses, the P2 line is critical in terms of series resistance losses.

Few likely loss scenarios related to the P2 Line are as follows:

(i) Too low laser fluence and incomplete removal of the active layer within the P2 line will cause an increase in the series resistance (R_s).
(ii) Too high laser fluence will cause damage to the ITO. Partially damaged ITO results in increased series resistance losses; completely damaged ITO will break the module interconnection.
(iii) A too narrow P2 line may again cause series resistance losses if the Ag/ITO interconnect is insufficient.
(iv) A too wide P2 line will cause GFF losses.

Losses (i) and (ii) can be properly addressed by a precise determination of the threshold power as well as of the overlap pattern. Losses (iii) and (iv) need to be examined at the hands of R_s and GFF losses in working solar modules and are sub-summarized under optimization of the P2 line. To address this optimization, we varied the width of the P2 patterning line from ≈30 µm (i.e., a single line) to ≈130 µm wide (i.e., multiple lines). Figure 6 and Table II compare the dark and illuminated *j*–V curves of reference cells with modules of different P2 line widths. Most importantly, all modules had roughly three times the open circuit voltage (V_{oc}) of the single cells. This is the first evidence that the laser patterning worked properly. Even more important is the observation that the module's fill factor (FF) was more or less identical to the single cells' FF. This is strong evidence that laser patterning of P1, P2, and P3 lines actually works without losses. The losses in the short circuit current (J_{sc}) are expected because it has a three times smaller single cell area in the module. Finally,

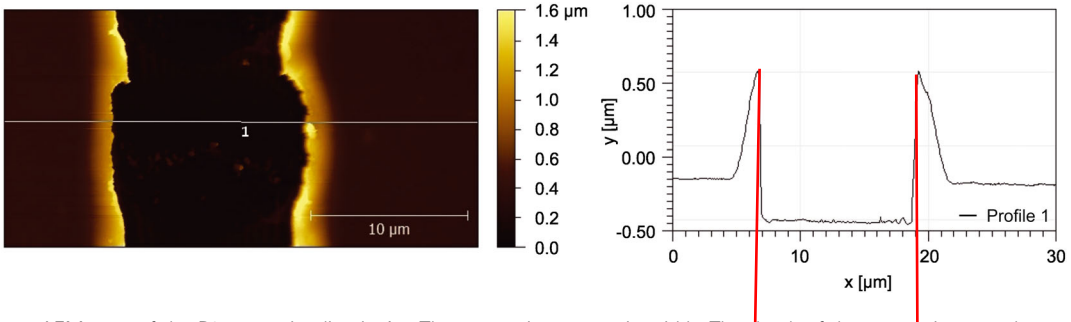

Figure 5. AFM scan of the P3 patterning line in Ag. The groove is 11.5 µm in width. The depth of the groove is more than 150 nm (evaporated Ag top electrode) suggesting that P3 patterning also removed parts of the underlying film. The protrusions on the side of the groove are strongly expressed and most likely consist of Ag (see microscope picture).

DOI: 10.1002/pip

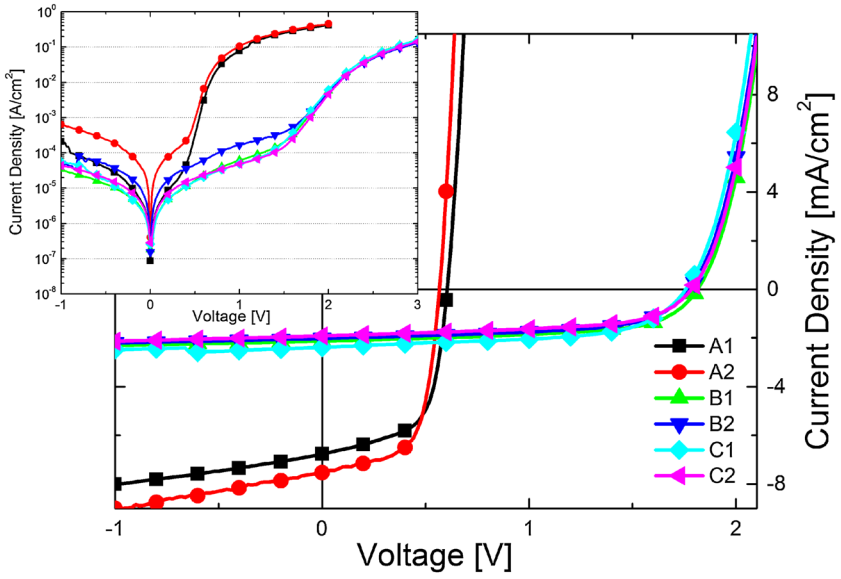

Figure 6. *j–V* characteristics of reference cells and modules. (A) Standard reference cells with the surface 10.4 mm^2; (B) modules consisting of three cells connected in series (surface of one cell less than one-third), P2 line patterning carried out with one single line; and (C) modules consisting of three cells connected in series (surface of one cell less than one-third), P2 line patterning carried out with multiple lines.

Table II. Performance of reference cells and modules.

	J_{sc} (mA/cm^2)	V_{oc} (V)	PCE (%)	FF (%)
A1	−6.78	0.60	2.50	61.57
A2	−7.54	0.57	2.71	63.05
B1	−2.13	1.81	2.33	60.42
B2	−2.02	1.78	2.15	59.91
C1	−2.38	1.76	2.45	58.48
C2	−1.92	1.78	1.99	58.37

Three times higher voltage of modules demonstrates the good functionality of each cell and interconnect.

J_{sc} is the short circuit current, V_{oc} the open circuit voltage, PCE stands for power conversion efficiency, and FF stands for fill factor.

by comparing the modules with 17- and 130-µm-wide P2 lines, it becomes clear that already 17-µm-wide ITO–Ag interconnection areas (P2 lines) are sufficient to guarantee a series resistance loss free current transport of approximately 10 mA/cm^2 (Table III). On the basis of this finding, all further modules were patterned with a single line for P2 (total width 30 µm; effective width 17 µm).

Table III. Comparison of fill factor and serial and parallel resistance of reference cells and the modules.

	FF (%)	R_s (Ω/cm^2)	R_p (kΩ/cm^2)
A1	61.57	3.10	42.18
A2	63.05	2.75	25.52
B1	60.42	4.78	11.90
B2	59.91	5.54	43.12
C1	58.48	4.46	2.48
C2	58.37	5.01	28.79

The device area in all cases was 10.4 mm^2.

To further demonstrate the potential of laser patterning for high GFF module manufacturing, we proceeded from three cell modules to 10 cell modules. A total area of only 115 mm^2 was selected for the 10-stripe modules, with each cell having approximately 11.5 mm^2 active area and a stripe width of 1 mm. This relatively small area was chosen to demonstrate the reproducibility of high resolution and the precision of laser patterning. All other processing parameters were taken over from the three-stripe modules. Figure 7 and Table IV summarize the data for the 10-stripe modules. This run shows somewhat lower performance of the reference cells, mainly due to a reduced J_{sc} and a slightly lower FF, which was caused by a thinner semiconductor layer (<180 nm) and large area. Nevertheless, comparing the reference with the module, we see that there are nearly no losses when processing modules out of cells. Overall, this is a further strong proof for the quality and the potential of laser patterning of organic solar cells. Figure 8 shows a picture of such a module as well as a magnified view of the interconnection regime. Best modules had a total interconnection regime of only 178 µm and a GFF of 83% (the contact pads are not included in GFF). This is a very good result, given that the total area of the 10-stripe module is only 115 mm^2 and is related to the high precision of the camera-based laser positioning system, which has a resolution of better than 50 µm. Further improvements in alignment and a further reduction of the laser fluence would expect us being able to reduce the interconnection width to less than 100 µm.

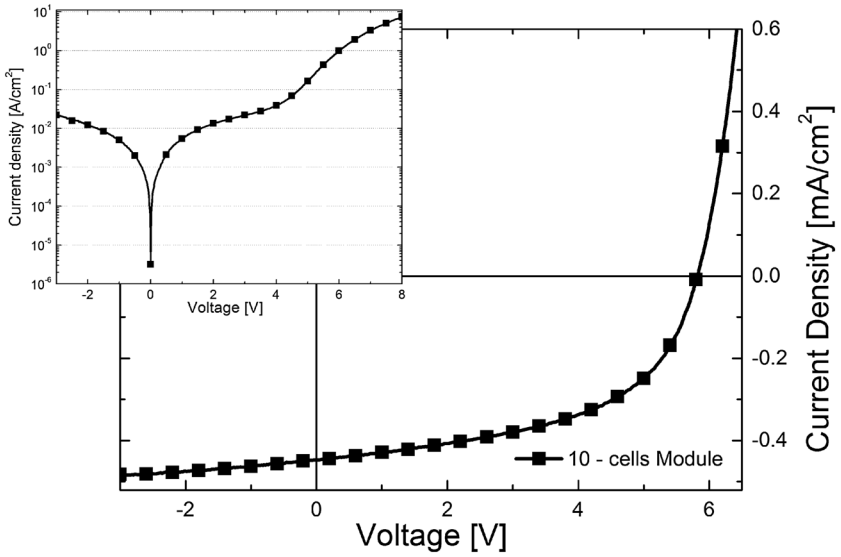

Figure 7. *j–V* characteristic of fabricated module consisting of 10 cells with an area of approximately 11.5 mm^2; the total area of the module counts for approximately 115 mm^2.

Table IV. Performance of the reference cell and 10 cells module.

	J_{sc} (mA/cm^2)	V_{oc} (V)	PCE (%)	FF (%)	Width of interconnection (μm)	GFF (%)
Reference cell	−5.18	0.59	1.71	56.06	n/a	n/a
Module	−0.45	5.82	1.38	52.88	180.15	83.20

We achieved a geometrical fill factor exceeding more than 83%.

PCE, power conversion efficiency; FF, fill factor; GFF, geometrical fill factor.

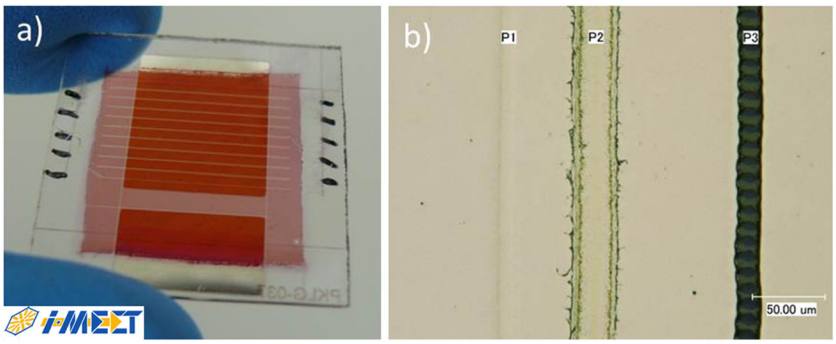

Figure 8. (a) Photos of the module and (b) the detail of interconnection area (1000× magnification) between two cells. In case of the larger module area and the same width of dead zone, the GFF can reach more than 98%.

While a GFF of 83% for a 10-stripe module is already impressive, scaling the module to slightly larger dimensions will directly result in even better GFF. An increase of the module area by only a factor 10 in width (i.e., from 10 to 100 mm width) and assuming the same interconnection width of 180 μm will immediately result in a GFF of more than 98%. Further reducing the interconnection area to 100 μm will allow reaching a GFF of 91% for a stripe width of 1 mm and total area of 115 mm^2.

4. CONCLUSION

In this manuscript, we introduced ultra short pulse laser patterning as an attractive method to produce glass-based modules with highest GFF. We demonstrated that patterning of all layers (P1, P2, and P3) can be realized with a single wavelength (520 nm), which is highly attractive from an economic point of view, and also relevant for integration of laser patterning into R2R processing. Only two

DOI: 10.1002/pip

processing parameters had to be optimized: the laser fluence and the patterning overlap. The formation of the protrusion at the sides of P2 and P3 patterning lines could be observed, the height profile being a function of the process parameters. However, these protrusions turned out to be uncritical because three-stripe as well as 10-stripe modules did not show electrical losses. According to Ben-Yakar *et al.*, protrusion formation can be suppressed with the increasing of the beam radius [24]. The use of a high-resolution, ultrafast laser patterning system allowed to produce modules with a GFF of 83% and lines out straightly the path to making modules with a GFF of over 98% at a laser speed of 4 m/s. Overall, short pulse laser patterning is outstanding in achieving precise ablation, fast processing, and an overall high GFF. Noteworthy to say that the aforementioned facts make this technology also attractive for all fields of organic electronics, which require fast processing and a high resolution in the tens of micrometer. As stable ultrafast laser patterning systems are available on the market, implementation of these systems in R2R production lines will allow OPV manufacturing with high throughput and excellent reproducibility.

ACKNOWLEDGEMENTS

The authors gratefully acknowledge the support of the EU-project X10D—"Efficient, low-cost, stable tandem organic devices," a collaborative project with 17 partners funded by the European Community's Seventh Framework Programme (FP7/2007-2013) under grant agreement no. 287818, the Cluster of Excellence "Engineering of Advanced Materials," and Energie Campus Nürnberg (EnCN).

REFERENCES

1. Press release, http://www.heliatek.com/ (May, 2012).
2. Press release, http://www.konarka.com/ (May, 2012).
3. Krebs FC. Fabrication and processing of polymer solar cells: a review of printing and coating techniques. *Solar Energy Materials and Solar Cells* 2009; **93**: 394–412.
4. Brabec CJ. Durrant JR. Solution-processed organic solar cells. *MRS Bulletin* 2008; **33**: 670–675.
5. Heise G, Dickmann M, Domke M, Heiss A, Kuznicki T, Palm J, Richter I, Vogt H, Huber HP. Investigation of the ablation of zinc oxide thin films on copper-indium-selenide layers by ps laser pulses. *Applied Physics A* 2011; **104**: 387–393.
6. Heise G, Domke M, Konrad J, Pavic F, Schmidt M, Vogt H, Heiss A, Palm J, Huber HP. Monolithical serial interconnects of large CIS solar cells with picosecond laser pulses. *Physics Procedia* 2011; **12**: 149–155.
7. Heise G, Heiss A, Hellwig C, Kuznicki T, Vogt H, Palm J, Huber HP. Optimization of picosecond laser structuring for the monolithic serial interconnection of CIS solar cells. *Progress in Photovoltaics: Research and Applications* 2012. DOI: 10.1002/pip.1261
8. Westin PO, Zimmermann U, Edoff M. Laser patterning of P2 interconnect via in thin-film CIGS PV modules. *Solar Energy Materials and Solar Cells* 2008; **92**: 1230–1235.
9. Westin PO, Zimmermann U, Ruth M, Edoff M. Next generation interconnective laser patterning of CIGS thin film modules. *Solar Energy Materials and Solar Cells* 2011; **95**: 1062–1068.
10. Choi HW, Farson DF, Bovatsek J, Arai A, Ashkenasi D. Direct-write patterning of indium–tin–oxide film by high pulse repetition frequency femtosecond laser ablation. *Applied Optics* 2007; **46**: 5792–5799.
11. Stegemann B, Fink F, Endert H, Schuele M, Schultz C, Quaschning V, Niederhofer J, Pahl HU. Novel concept for laser patterning of thin film solar cells. *Laser Technik Journal* 2012; **9**: 25–29.
12. Matylitsky VV, Kubis P, Brabec CJ, Aus der Au J. High Q femtoREGEN^{TM} UC laser systems for industrial micro-processing applications. *SPIE Proceedings* 2012. DOI: 10.1117/12.906750
13. Matylitsky VV, Huber H, Kopf D. Selective removal of transparent conductive oxide layers with ultra short laser pulses: front- vs. back-side ablation, International Congress on Applications of Lasers and Electro-Optics Paper M903 (2011) 1022–1027.
14. Chichkov BN, Momma C, Nolte S, Alvensleben F, Tuennermann A. Femtosecond picosecond and nanosecond laser ablation of solids. *Applied Physics A* 1996; **63**: 109–115.
15. Korte F, Adams S, Egbert A, Fallnich C, Ostendorf A, Nolte S, Will M, Ruske JP, Chichkov B, Tuennermann A. Sub-diffraction limited structuring of solid targets with femtosecond laser pulses. *Optics Express* 2000; **7**: 41–49.
16. Chien CY, Gupta MC. Pulse width effect in ultrafast laser processing of material. *Applied Physics A* 2005; **81**: 1257–1263.
17. Ancona A, Roeser F, Rademaker K, Limpert J, Nolte S, Tuennermann A. High speed laser drilling of metals using a high repetition rate, high average power ultrafast fiber CPA system. *Optics Express* 2008; **16**: 8958–8968.
18. Baerenklau M, Muhsin B, Moreno JG, Roesch R, Horn A, Gobsch G, Stute U, Hoppe H. Polymer solar modules: laser structuring and quality control by lock-in thermography. *MRS Proceedings* 2012; **1390**. DOI: http://dx.doi.org/10.1557/opl.2012.648
19. Moreno JG, Baerenklau M, Schoonderbeek A, Muhsin B, Haupt O, Roesch R, Gobsch G, Teckhaus D, Hoppe H, Stute U. Thin-film organic solar modules – processing

and laser ablation. *EU PVSEC Proceedings* 538–542. DOI: 10.4229/26thEUPVSEC2011-1DV.3.13

20. Stubhan T, Litzov I, Li N, Salinas M, Steidl M, Sauer G, Matt GJ, Halik M, Brabec CJ. Overcoming interface losses in organic solar cells by applying low temperature, solution processed aluminum doped zinc oxide electron extraction layer, Article in preparation.
21. Heise G, Domke M, Konrad J, Sarrach S, Sotrop J, Huber HP. Laser lift-off initiated by direct induced ablation of different metal thin films with ultra-short laser pulses. *Journal of Physics: Applied Physics* 2012; **45**: 315303–315311.
22. Ben-Yakar A, Byer RL. Femtosecond laser ablation properties of borosilicate glass. *Journal of Applied Physics* 2004; **96**: 5316–5323.
23. Xiao S, Fernandez SA, Ostendorf A. Selective patterning of ITO on flexible PET substrate by 1064 nm picosecond laser. *Physics Procedia* 2011; **12**: 125–132.
24. Ben-Yakar A, Harkin A, Ashmore J, Byer RL, Stone HA. Thermal and fluid processes of a thin melt zone during femtosecond laser ablation of glass: the formation of rims by single laser pulses. *Journal of Physics D: Applied Physics* 2007; **40**: 1447–1459.